

Ultrafast X-ray Spectroscopy of Intersystem Crossing in Hexafluoroacetylacetone: Chromophore Photophysics and Spectral Changes in the Face of Electron Withdrawing Groups

Eric A. Haugen,^{†,‡} Diptarka Hait,^{†,‡} Valeriu Scutelnic,^{†,‡} Tian Xue,^{†,‡} Martin Head-Gordon,^{†,‡} and Stephen R. Leone^{*,†,‡,¶}

[†]*Department of Chemistry, University of California, Berkeley, CA 94720, USA*

[‡]*Chemical Sciences Division, Lawrence Berkeley National Laboratory, Berkeley, CA 94720, USA*

[¶]*Department of Physics, University of California, Berkeley, CA 94720, USA*

E-mail: srl@berkeley.edu

Abstract

Intersystem crossings between singlet and triplet states represent a crucial relaxation pathway in photochemical processes. Herein, we probe the intersystem crossing in hexafluoro-acetylacetone with ultrafast X-ray transient absorption spectroscopy at the carbon K-edge. We observe the excited state dynamics following excitation with 266 nm UV light to the $^1\pi\pi^*$ (S_2) state with element and site-specificity using a broadband soft X-ray pulse produced by high harmonic generation. These results are compared to X-ray spectra computed from orbital optimized density functional theory methods. It is found that the electron withdrawing fluorine atoms decongest the X-ray absorption spectrum by enhancing separation between features originating from different carbon

atoms. This facilitates the elucidation of structural and electronic dynamics at the chromophore. The evolution of the core-to-valence resonances at the carbon K-edge reveals an ultrafast population transfer between the $^1n\pi^*$ (S_1) and $^3\pi\pi^*$ (T_1) states on a 1.6 ± 0.4 ps timescale, which is similar to the 1.5 ps timescale earlier observed for acetylacetone [J. Am. Chem. Soc. **139**, 16576 (2017)]. It therefore appears that terminal fluorination has little influence on the intersystem crossing rate of the acetylacetone chromophore. In addition, the significant role of hydrogen-bond opened and twisted rotational isomers is elucidated in the excited state dynamics by comparison of the experimental transient X-ray spectra with theory.

Introduction

Light induced chemical reactions possess the ability to redistribute energy over various electronic states and initiate changes in molecular geometry. This redistribution of energy plays a key role in a wide variety of molecular systems ranging from biological, atmospheric/interstellar, molecular switches and many more.¹⁻⁴ Fundamental understanding of the relationship between nuclear and electronic motion continues to be a primary driving force for scientific studies that seek to describe photochemistry on an ultrafast timescale.

The goal of creating a “molecular movie”, which provides a clear step-by-step picture of both the electronic and nuclear dynamics on the timescales of nuclear motion, remains attractive in the field of physical chemistry. In order to pursue this goal, numerous techniques and methods have been employed, including photoelectron spectroscopy, X-ray absorption spectroscopy, electron diffraction and many other methods, all aiding in providing a clearer picture of the dynamics following photoexcitation.⁵⁻⁷ As the fundamental understanding of standard systems grows, there will be increased demand to selectively modify molecular systems in order to fine-tune various chemical properties for use in future devices or applications. Of particular interest is acetylacetone (AcAc), which is a prototypical molecule that has been studied in depth to elucidate the ultrafast intersystem crossing between sin-

plet and triplet states.⁸⁻¹⁰ The AcAc structure has many possible industrial, medical and environmental uses, as it can act as a chelating agent or serve as a structural component for UV-chromophores.¹¹⁻¹³

Controlling the rate of the transition between the singlet and triplet states can be used to influence the quantum efficiency of various relaxation pathways, ultimately favoring certain channels over others. One potentially significant modification to AcAc is the substitution of the CH₃ groups with CF₃ groups, as shown in Fig. 1.

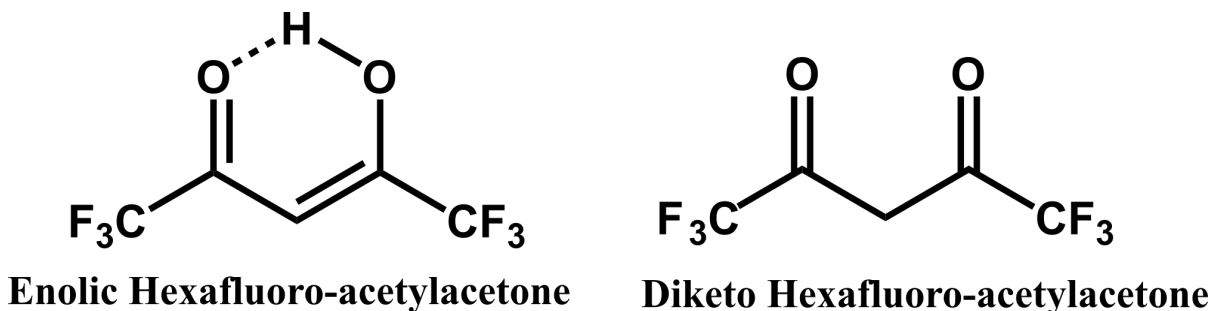


Figure 1: Structures of the enolic and diketo tautomers of hexafluoro-acetylacetone. The enolic form is more stable and is present as the dominant tautomer under experimental conditions.

The CF₃ functional groups are strongly electron withdrawing and have been shown to exert a large influence on molecules, resulting in markedly different photoproducts and chemical properties.¹⁴⁻¹⁷ However, the fluorine substituted hexafluoro-acetylacetone (HfAcAc) has, to our knowledge, not previously been studied in the ultrafast regime. It is thus unknown to what extent the terminal CF₃ groups might influence the electronic state dynamics of the main chromophore of the molecule. Notably, in some conjugated chromophores it has been shown that the addition of fluorine atoms has the ability to influence the energies of the various electronic states of the molecule, thereby affecting the rate of intersystem crossing.^{18,19} The ability to fine-tune quantum yields of various processes is attractive for optical imaging applications or other processes such as maximizing singlet oxygen generation. Additionally, greater understanding of the mechanisms underlying intersystem crossings can prove useful for applications such as thermally activated delayed fluorescence organic light

emitting diodes, where great care is taken to fine-tune the conversion between singlet and triplet states.^{20,21} Due to these considerations, there is an ever-increasing importance to fundamentally understand how modifying functional groups influences the various pathways corresponding to relaxation of excited electronic states.

The photodynamics of HfAcAc can be contrasted with AcAc; here the six additional fluorines act as electron withdrawing groups, heavily favoring the enol hydrogen-bonded “ring” form of the well known keto-enol equilibrium in β -diketones.¹⁷ However, the strong intramolecular hydrogen bond is believed to be significantly weakened by the terminal CF_3 groups.^{22,23} Indeed, we computationally find that the hydrogen bond in HfAcAc is weaker by 5 kcal/mol than AcAc (as detailed in the supporting information). It is therefore easier to break the hydrogen bond in HfAcAc, thereby permitting rotation of the O-H bond about the enol C-O bond, potentially allowing different excited state dynamics to occur following electronic excitation, in this case with 266 nm light.

Table 1: Vertical electronic excitation energies (in eV) at the ground state minimum geometry for HfAcAc and AcAc, as computed from TDDFT with $\omega\text{B97X-D/aug-pcseg-1}$. n refers to the lone pair on the keto oxygen.

| State | Character | HfAcAc | AcAc |
|-------|--------------|--------|------|
| T_1 | $^3\pi\pi^*$ | 2.93 | 3.31 |
| T_2 | $^3n\pi^*$ | 3.73 | 4.04 |
| S_1 | $^1n\pi^*$ | 4.21 | 4.46 |
| S_2 | $^1\pi\pi^*$ | 5.04 | 5.21 |

The UV absorption spectra of both AcAc and HfAcAc share many similarities, both possessing strong and broad $\pi \rightarrow \pi^*$ transitions around 266 nm corresponding to excitation into the S_2 state.^{24,25} Indeed, calculations reveal that the four lowest excited states have similar energies and character in the Franck-Condon (FC) region, as shown in Table 1. It is therefore expected that both species will ultimately undergo intersystem crossing into the T_1 state following excitation to S_2 , before relaxing to the ground state or dissociating. The possible role of the T_2 state is not known and is not explored here. The additional fluorines allow for a greater variety of potential photoproducts in HfAcAc, permitting the production

of pentafluoromethyl-3-furanone together with HF in the low pressure regime.^{14,26,27} The proposed pathway to this photoproduct relies on the cleavage of the intramolecular O-H hydrogen bond, thereby allowing the molecule to rotate and form a series of rotationally distinct isomers. These rotational isomers can act as precursors to the aforementioned photoproducts. Observation of these dynamics on ultrafast timescales is desirable to define the initial steps that the primary chromophore undergoes. In particular transient X-ray absorption spectroscopy will allow for the clear demarcation of the various singlet and triplet states from one another and can detect any potential photoproducts that might arise from the parent molecule.^{10,28}

The field of transient X-ray absorption spectroscopy (Tr-XAS) with femtosecond timescales has made steady progress in recent years; tabletop sources producing soft X-rays via high harmonic generation have improved allowing experiments in the water window to be performed.²⁹⁻³² Tr-XAS is a powerful technique that acts as a probe for both the electronic and structural dynamics of molecules. The X-rays provide unique element specificity due to the transitions originating from localized core orbitals, and the energies corresponding to these transitions for each element vary between atoms in different locations in the molecule, resulting in spectra with site specificity. Thus core-level transitions are sensitive to the local chemical environment and report on shifts in electron density in the proximity of the probed atoms.³³ Here, we use femtosecond soft X-ray transient absorption spectroscopy to probe the ultrafast non-adiabatic population transfer into the triplet $^3\pi\pi^*$ (T_1) state following the initial excitation of ground state HfAcAc to the optically bright $^1\pi\pi^*$ (S_2) state, thereby gaining insight into the photochemical reaction pathways.

We compare the results to previous measurements on AcAc and computed spectra obtained via orbital optimized density functional theory methods.³⁴ The results show that the rate of the non-adiabatic passage to the T_1 state in HfAcAc is not significantly influenced by the terminal fluorine atoms while providing clear evidence for hydrogen-bond ring opened and twisted rotational conformers in the excited state dynamics, in contrast to the initial

hydrogen bonded, planar, enol form in the ground state.

Methods

Experimental

HfAcAc (98% purity) purchased from Sigma Aldrich was stored in glass vials under refrigeration. No further purification of the samples was undertaken. The sample container was submerged in an ice-salt bath at approximately -5° C. The HfAcAc was probed using a gas cell with a path length of 4 mm and an approximate pressure of ≈ 15 mbar. This gas cell was further heated to 60° C to reduce clogging.

A comprehensive description of the experimental setup may be found in previous papers.^{10,29,35,36} Briefly, a commercial Ti:Sapphire laser (Spit-fire Ace, Spectra Physics) provides a 12mJ, 1kHz, sub-45fs pulse duration output. This pulse was split by a 90:10 beam-splitter where 10% is used to generate the UV pump and 90% pumps an optical parametric amplifier (HE-TOPAS, Light Conversion, 1180-2600 nm). The optical parametric amplifier was tuned to produce 1470 nm (2.5-3.0 mJ/pulse) with a duration of ≈ 50 fs. The 1470 nm pulse was used to generate a broadband soft X-ray pulse extending to the carbon K-edge (160-350 eV, sub 50 fs), which will act as the probe. The soft X-rays were focused with a gold toroidal mirror onto the sample and subsequently dispersed with an XUV variable line space grating with 1200 lines/mm (Hitachi grating 001-0660) onto a translatable X-ray camera (Princeton Instruments, PIXIS:XO 400B). The ultraviolet pump was generated from the remaining 10% output from the Ti:Sapphire laser in a two-step process consisting of second harmonic generation resulting in production of 400 nm and sum frequency generation (SFG) of 800 and 400 nm resulting in the generation of a sub 70 fs, 266 nm pulse with a maximum energy of $120 \mu\text{J}/\text{pulse}$, this pulse energy was detuned by rotating the SFG BBO to limit the energy to no more than $40 \mu\text{J}/\text{pulse}$. The HfAcAc molecules were excited with the 266 nm pulses with up to $\sim 30 \text{ mJ}/\text{cm}^2$ pump fluence ($2.5 \times 10^{11} \text{ W}/\text{cm}^2$ intensity). The molecular

dynamics were then probed with the broadband, soft X-ray pulse optimized for flux at the carbon K-edge at varying time delays between the pump and probe pulses.

The time delays utilized in this experiment were increased by increments of 100 fs between time zero and 500 fs, 250 fs between 500 fs and 4 ps, and 2.5 ps between 4 ps and 20 ps. A final delay point of 30 ps is also measured. Recent experiments indicate an instrument response function of ≈ 80 fs.²⁹ This is determined by an *in situ* cross-correlation of the pump and probe pulses through measurement of the ponderomotive shift of the core-excited Rydberg states of argon. The X-ray spectral resolution of the experiment is determined to be 320 ± 30 meV through measurement of the Gaussian broadening of the $2p_{3/2} \rightarrow 4s$ transition in argon, assuming a core-hole lifetime broadening of 114 meV³⁷ (Fig. S1).

Theoretical

All calculations are performed with a development version of the Q-Chem 5 package.³⁸ C K-edge spectra are simulated with excited state specific orbital-optimized DFT (OO-DFT³⁴), utilizing the SCAN functional.³⁹ In particular, the spectra of closed-shell species are modeled with restricted open-shell Kohn-Sham (ROKS^{40,41}), with initial guesses generated from the recently developed static exchange approximation to ROKS [ROKS(STEX)] approach.⁴² The spectra of open-shell systems are computed via Δ SCF.^{43,44} Naive Δ SCF calculations yield spin-impure results when both unpaired up and down spins are present, but approximately spin-pure results can be obtained through use of the general recoupling procedure described previously.^{34,45} ROKS and recoupled Δ SCF, with the SCAN functional, have been previously found to be accurate to ~ 0.3 eV in predicting C K-edge excitation energies against experiment,^{45,46} without any need for empirical translation of spectra. OO for electronic excited states are performed with the square gradient minimization (SGM⁴⁷) and initial maximum overlap method (IMOM⁴⁸) algorithms, for restricted open-shell and unrestricted calculations, respectively. A mixed basis-set of aug-pcX-2⁴⁹ at the site of the core-excitation, and aug-pcseg-1⁵⁰ on all other atoms is utilized for C K-edge calculations.⁴⁵⁻⁴⁷

Geometries are optimized at the ω B97X-D⁵¹/aug-pcseg-1 level, with this functional being chosen as it yields good performance for excited states.⁵² The S_0 and T_1 states are optimized with standard ground state DFT within the singlet and triplet subspaces, respectively. The S_1 state is optimized with time-dependent DFT (TDDFT), without the Tamm-Dancoff approximation (TDA).⁵³ The minimum energy crossing point (MECP) between the S_2 and S_1 states is determined at the same level of theory. TDDFT is not employed for the T_1 state, as the equilibrium structures of some rotamers in this state involve breaking of a π bond, which TDDFT (or TDA) is incapable of modeling.⁵⁴

Results and Discussion

Ground State

Fig. 2 shows the experimental near-edge X-ray absorption fine structure (NEXAFS) spectrum of HfAcAc in the S_0 (ground) state, (blue points and solid blue line with error bars). The computed ROKS C K-edge spectrum for the enol tautomer is also shown. The stick spectrum displays calculated core-valence transitions of the constituent carbon atoms underlying the peaks in the observed NEXAFS spectrum. The individual computed peaks are broadened by 0.3 eV to produce the shaded grey spectrum. It can be clearly seen that the transitions corresponding to distinct groups of carbon atoms are significantly shifted from one another and are most prominent in their own distinct region of the X-ray spectrum. This shift arises from a chemical shift of the binding energy of the core $1s$ electrons due to their proximity to more electronegative heteroatoms. OO-DFT calculations indicate that the C_3 atom has the lowest $1s$ binding energy (i.e. core ionization energy) at 291.7 eV, the oxygen bound C_2 and C_4 atoms have $1s$ binding energies of 294.3-294.5 eV, while the C_1 and C_5 atoms directly bound to the fluorines have $1s$ binding energies of 298.7-299.1 eV. This is reflected in the X-ray absorption spectrum for the lowest energy $1s \rightarrow \pi^*$ (LUMO) transitions. The central C_3 atom has the lowest energy transition at 284.4 eV, while C_2 and

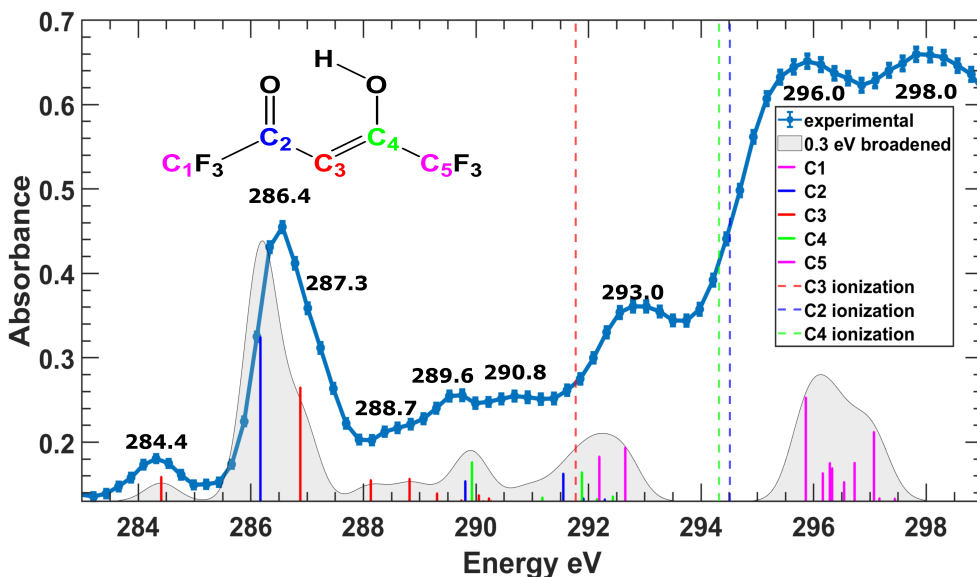


Figure 2: Experimentally measured, near-edge X-ray absorption fine-structure (NEXAFS) spectrum of HfAcAc (S_0) at the carbon K-edge (solid blue line, error bars denotes 95% confidence interval) with the main peaks annotated. The calculated ROKS spectrum of the enol tautomer is shown as a stick spectrum, color coded for distinct carbon atoms present in the molecule. The grey shaded feature corresponds in the stick spectrum broadened with a $\sigma=0.3$ eV width Gaussian. The intensity of the theoretical spectrum is uniformly scaled to match experiment for the strong absorption feature at 286.4 eV. The calculations do not take into account the core- $1s$ ionization, which increases with increasing energy. The rising edge at ~ 292 eV corresponds to ionization from C_3 , while the rising edge at ~ 294 eV arises from ionization from C_2 and C_4 . The dotted lines correspond to the calculated ionization energies, the ionization energy for C_1 and C_5 are present at ~ 299 eV.

C_4 start absorbing around 286.4 eV.

The effect of the fluorine atoms on the $C_2/C_3/C_4$ $1s \rightarrow \pi^*(\text{LUMO})$ excitation energies appears to be nearly negligible with a maximum of a 0.2 eV shift compared to the results of acetylacetone found by Bhattacharjee *et al.*¹⁰ This minor effect indicates that the presence of the electronegative heteroatoms does not significantly affect the relative spacing between the core and the unoccupied valence levels in neighboring atoms, with excitation energies being significantly affected only for the atom to which the electronegative heteroatoms are bonded to. However, a large shift of around 4.8 eV for the lowest excitation out of C_1 and C_5 is found to arise from the substitution of hydrogen with fluorine. This large blue shift greatly simplifies the spectrum and helps distinguish between transitions from the

terminal and central carbon atoms. Furthermore, computationally the additional fluorine atoms increase the lowest core-ionization potential of the entire molecule (corresponding to C_3) by almost 1.6 eV compared to what is observed experimentally in AcAc.¹⁰ In HfAcAc the C_3 carbon is calculated to have the lowest vertical ionization potential at 291.7 eV, while the corresponding value for AcAc is 290.1 eV. As a result, transitions above 289 eV in AcAc, are unable to be resolved experimentally due to the onset of ionization of C $1s$ electrons.¹⁰ Similarly, the lowest vertical valence ionization energy for HfAcAc is computed to be 10.63 eV, while it is 9.05 eV for AcAc. With only minor shifts observed in the $1s \rightarrow \pi^*$ (LUMO) transition for the C_2 , C_3 and C_4 atoms, it therefore appears that the influence of the fluorine atoms is primarily to lower the energies of core and valence levels associated with the central chromophore (C_2 , C_3 and C_4) by roughly the same amount (1.6 eV) relative to an orbital infinitely far away (i.e. the continuum). Consequently, electrons are more strongly bound against ionization in HfAcAc relative to AcAc, while the excitation energies for core-to-valence or valence-to-valence transitions are relatively unaffected (as illustrated by the core-level excitation energies discussed in the text and Table 1 for valence excitations). This greatly increases the range where core-level X-ray transitions may be clearly observed prior to the onset of the core-ionization continuum, allowing significantly more transitions to be experimentally detected.

The $1s \rightarrow \pi^*$ (LUMO) excitations from C_1 and C_5 are predicted to only begin at ~ 292.2 eV (obscured in the experimental spectrum by the C_3 ionization edge), which leads to a prominent peak at 293.0 eV. We note that the C_1 and C_5 atoms have significant oscillator strength for these transitions only because there exist C-F σ^* levels of the same orientation as the π^* (LUMO). The separation between these unoccupied levels is too large in the ground state molecule for any mixing of character, as made evident by the similar core-excited state energies for HfAcAc and AcAc for the chromophore centered excitations that were previously described. However, a core-hole centered at C_1 or C_5 would stabilize the local C-F σ^* levels to a significantly greater extent than the π^* centered on the chromophore, through reduced

electronic repulsion. This permits mixing of C-F σ^* character into the π^* LUMO for core-level X-ray transitions out of C₁ and C₅, leading to some oscillator strength for the $1s \rightarrow \pi^*$ transitions. This behavior is therefore different from the stabilization of core and valence chromophore orbitals by core-hole free CF₃ moieties that were described earlier.

The shoulder in the S₀ spectrum at ~ 287 eV can be solely assigned to the C₃ $1s \rightarrow \pi^*(\text{LUMO}+1)$ transition. The broad region at ~ 288.7 eV arises from C₃ $1s$ as well, corresponding to excitations to σ^* and Rydberg levels. Higher energy peaks observed, such as at 289.6 and 290.8 eV, correspond to a mixture of overlapping transitions of the $1s$ core-electrons of C₂, C₃ and C₄ to higher energy unoccupied valence and Rydberg orbitals. Improved experimental resolution would be needed to distinguish between the transitions and to assign them to distinct carbon atoms. Finally, the peaks at 296.0 and 298.0 eV correspond to transitions of the CF₃ carbons and are composed of numerous excitations to higher unoccupied valence and Rydberg orbitals.

It should be noted that previous studies on HfAcAc¹⁷ have demonstrated that the enolic tautomer will be the dominant configuration of HfAcAc with $> 99\%$ contribution under current experimental conditions. Due to this, the contribution of the diketone tautomer of the HfAcAc is negligible and its effect on the ground state spectrum was not considered.

As noted earlier, the substitution of CF₃ type carbons for CH₃ carbons pushes the transitions associated with those carbon atoms to higher energies and allows for the clear distinction between the terminal carbons $1s \rightarrow \pi^*$ and the central carbons $1s \rightarrow$ Rydberg transitions. This allows greater distinction between the carbon peaks of HfAcAc, allowing them to be more clearly defined and isolated from one another. This demonstrates the possibility of adding strong electron withdrawing groups to complex systems in future experiments to help isolate and deconvolute electronic transitions at the carbon K-edge.

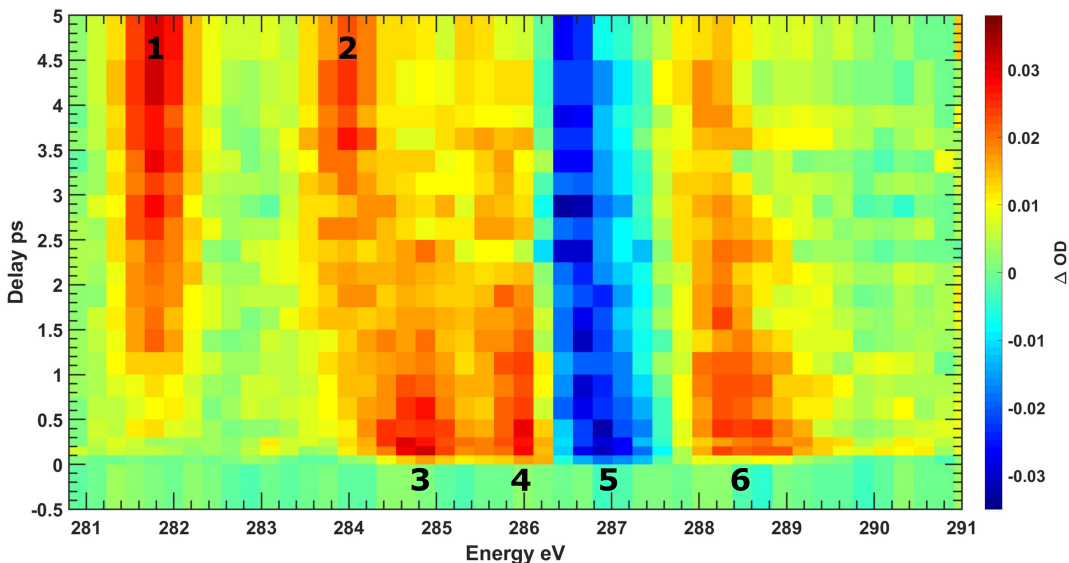


Figure 3: Experimentally measured, transient spectrum versus time of HfAcAc following excitation with 266 nm pump pulse.

Excited State Dynamics

Fig. 3 shows a two-dimensional false color transient differential absorption map of the transient C K-edge X-ray spectrum of HfAcAc after excitation with a 266 nm UV pulse for time delays of -500 fs to 5 ps. All experimental signals correspond to a single photon excitation, as may be seen in Fig S2. Data taken at longer time delays do not significantly deviate from the 5 ps results (as shown in Fig. S5). The red-yellow and blue colors represent positive and negative ΔOD features, respectively. Here the pump-off spectrum was used to determine the correlation matrix that was employed for the edge-pixel referencing technique, reducing noise originating from fluctuations in the high harmonic generation process which is present in transient absorption data.⁵⁵

Six easily distinguishable features are seen in Fig. 3, which are labeled 1-6. OO-DFT calculations and comparison to previous results for AcAc¹⁰ indicate that several of these features can be assigned to the ${}^1n\pi^*$ (S_1) and ${}^3\pi\pi^*$ (T_1) states (where n corresponds to the non-bonding 2p lone pair on the ketone O atom). The intersystem crossing between these states occurs in 1.6 ± 0.4 ps, as discussed later.

OO-DFT calculations reveal that peaks 1 and 2 (281.7, 283.9 eV) correspond to the T_1 state, while peaks 3 and 4 (284.8, 285.9 eV) correspond to the S_1 state. Peak 5 corresponds to the depleted S_0 state and is centered at 286.3 eV. An energy shift on the right shoulder of the ground state depletion at increasing delays indicates a transition from singlet to triplet states. Peak 6 (288.6 eV) likewise corresponds to the S_1 and T_1 states, where a clear energy shift occurs, corresponding to passage through the intersystem crossing. Higher energy transient signals seemingly unrelated to the aforementioned intersystem crossing are also present. These transitions will primarily arise from the terminal CF_3 carbons, which are discussed further in the supporting information.

The transient data at energies below the primary ground state depletion shows very similar characteristics to that of AcAc. The energies of low energy peaks assigned to the triplet T_1 state and the singlet S_1 state (281.7, 283.9, 284.8, 285.9 eV, respectively) are very similar to the corresponding energies found for AcAc by Bhattacharjee *et al.*¹⁰ (281.4, 283.8, 284.7, 285.9 eV, respectively). These low energy features are a result of transitions originating from the central chromophore consisting of C_2 , C_3 , C_4 , which are identical for both molecules. This is analogous to what was observed in the ground state static spectrum where the presence of the fluorines did not strongly affect core-excitation energies from C_2 , C_3 , C_4 . As with the ground state, higher energy features can be clearly resolved owing to the blueshift of excitations/ionizations corresponding to the terminal CF_3 carbons. In particular, peak 6 (which is higher in energy than the ground state bleach) does not have an analogue in the unsubstituted AcAc transient spectrum.

Fig. 4 shows experimental transient XAS spectra at selected time delays that convey the clear energy shift due to the $S_1 \rightarrow T_1$ intersystem crossing. Here 100 fs represents primarily S_1 character, 1 ps represents a mixture of S_1 and T_1 , and 5 ps represents primarily T_1 character. The -500 fs timepoint is also presented as a reference for the intrinsic noise of the experiment, as it should ideally have $\Delta OD = 0$ throughout. In this figure a clear transition between the features of the singlet and triplet can be distinguished. All time delays longer

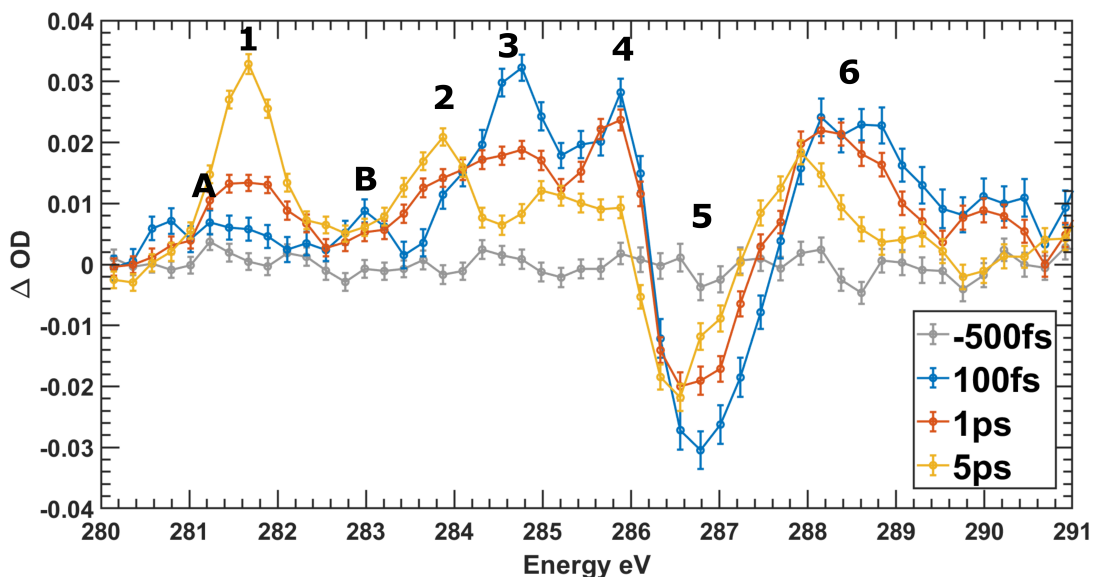


Figure 4: ΔOD at 100 fs, 1 ps, and 5 ps illustrating the shift from the singlet S_1 state to the triplet T_1 state. Peaks 1-6 correspond to the transitions observed in Fig. 3, meanwhile transitions A and B correspond to weak $1s \rightarrow n$ (singly occupied oxygen 2p lone-pair) transitions consistent with the S_1 state, on the basis of OO-DFT calculations.

than 5 ps did not reveal any further significant changes in the spectrum, indicating that the triplet state is long-lived up to at least 30 ps and that photodissociation of HfAcAc occurs on a longer timescale. Longer time delays are observed in the supplement in Fig. S5. In addition to features 1-6, weak peaks at 281.2 and 283.0 eV in the 100 fs trace are labeled as features A and B, respectively. These weak peaks correspond to excitations to the singly occupied oxygen 2p lone-pair (n) orbital in the S_1 state. The aforementioned assignments will be justified below through the comparison of the experimental results with the theoretical calculations.

Fig. 5 illustrates the theoretical excited state spectra for the S_1 state at two geometries and two rotational isomers (rotamers) of the T_1 state, with the experimental spectrum for both states taken at two different time delays. In Fig. 5, the different color bars correspond to the different carbon atoms and the shaded grey spectrum corresponds to a 0.3 eV broadened spectrum. The blue traces correspond to the excited state spectrum obtained via the addition of the static S_0 spectrum to the transient resolved spectra, assuming a 20% excitation from

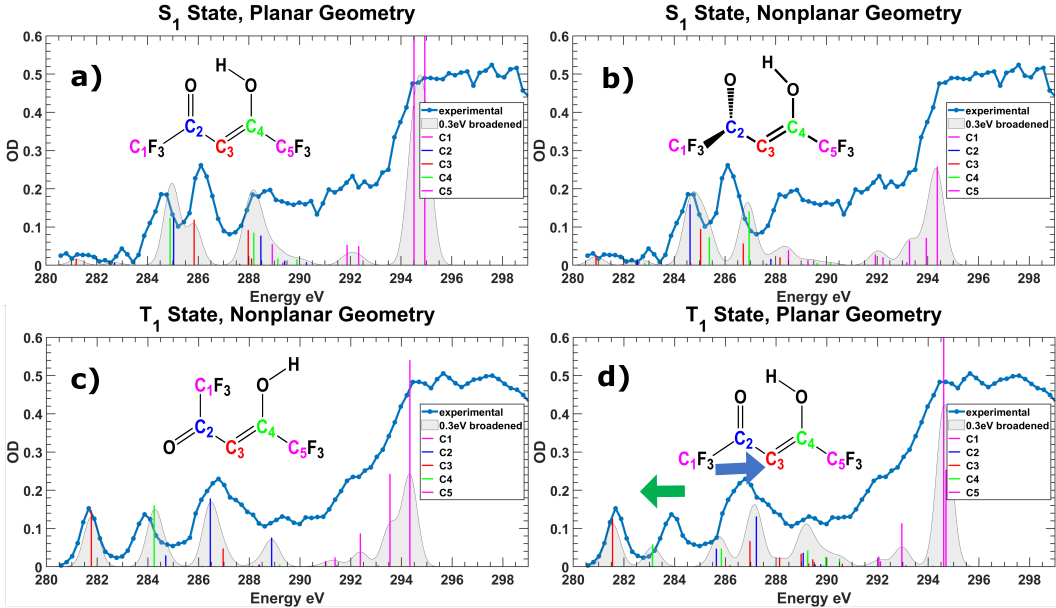


Figure 5: Experimentally determined S_1 and T_1 states compared with OO-DFT calculations. The timepoint of 100 fs was chosen as the experimental S_1 state and timepoints from 5-30 ps were averaged for the experimental T_1 state. a) S_1 electronic state at its optimized geometry, where the π system ($O=C_2C_3C_4$) is planar (0.0° dihedral). b) S_1 electronic state at the geometry of the S_2/S_1 MECP geometry where a 34.4° dihedral angle is present in π system ($O=C_2C_3C_4$). c) T_1 electronic state for rotational isomer with a broken hydrogen bond, which permits free rotation. d) T_1 electronic state with a planar structure with the intramolecular hydrogen bond still intact. Arrows are included in d) to highlight predicted energy shifts for the calculated low-energy C_2/C_4 transitions, driven by changes from non-planar to planar geometry.

the ground state (which is the minimum fraction required to avoid any unphysical negative absorbance in the excited state spectrum, which may arise from an improper subtraction the ground state signal). The geometries corresponding to these excited states are provided in the supporting information. Additional computed XAS for the S_2 , S_1 , and potential photoproducts are also shown in Fig. S6.

Briefly, the calculated $^1\pi\pi^*$ (S_2) state spectrum in the unrelaxed (Franck-Condon) geometry is predicted to have relatively strong “fingerprint-like” features at 280.3 and 282.1 eV arising from transitions to the singly occupied π bonding (HOMO-1) level, which are not observed in the experimental data. Indeed, no obvious rapid changes in ΔOD , indicative of changing the electronic state, are observed in short time scans between 0 and 100 fs (as

depicted in Fig. S7). This indicates that the internal conversion between the S_2/S_1 states occurs on a timescale faster than the temporal resolution of the experiment (~ 80 fs). Likewise, it is unknown whether the intersystem crossing follows El-Sayed’s rules (corresponding to a direct $S_1 \rightarrow T_1$ transition) or if the T_2 state acts as a very short-lived intermediate form.^{8,10} Nevertheless, it is expected that the lifetime of the T_2 state would be too short to build up any significant population before relaxing to the T_1 state, thus rendering it difficult to experimentally observe it with our setup.

Fig. 5a) demonstrates the comparison between the experimental data at 100 fs and the OO-DFT computed spectra of the S_1 state at the optimized global minimum, planar geometry for this state. Clear discernible features at 281.2, 283.0, 284.6, 286.1 and 288.5 eV are observed in the experimental data, with higher energy features also present. The OO-DFT calculated spectrum predicts the first two, relatively weak, peaks of the spectrum, which arise from $1s \rightarrow n$ transitions from C_3 and $C_{\{2,4\}}$ respectively. However, the theory underestimates the strength of the second peak and slightly shifts the predicted energy of the second peak to 282.7 eV. The strong experimental peak at 284.6 eV can be assigned to calculated $1s \rightarrow \pi^*$ transitions from C_2 and C_4 at 285.0 eV and 284.9 eV. A relatively strong excitation from C_3 is predicted at 285.8 eV. The corresponding experimental feature is at 286.1 eV, which is perceptibly more intense than what is predicted by theory. The higher energy feature at 288.5 eV is predicted by the OO-DFT calculations to correspond to other transitions from central carbon atoms.

Fig. 5b) compares the same 100 fs experimental data to the computed OO-DFT spectrum for the S_1 state at the S_2/S_1 MECP geometry. Notably this configuration possesses a large dihedral angle of approximately 34° for the central three carbon atoms and the carbonyl oxygen. This deviation from planarity is driven by the $\pi\pi^*$ character present in the S_2 state, which allows easy deformation of the planar π system. The computed spectrum at this geometry shows significant differences from the spectrum computed for the $S_{1\text{min}}$ geometry shown in Fig 5 a), particularly in the range of 284.5-289 eV. The strong feature at 288.5

eV is absent, while there is a greater splitting in the predicted $1s \rightarrow \pi^*$ transitions, seen experimentally at 284.6 eV and 286.1 eV.

These differences arise from the nonplanarity of the molecule in this geometry, which leads to significant changes to the π orbital system. It is worth noting that the experimental 286.1 eV signal lies between the corresponding peaks computed at the planar global minimum geometry in 5a) and the nonplanar geometry in 5 b). This suggests that the 100 fs experimental spectrum is probably best described by an ensemble of possible molecular geometries in the S_1 state. Indeed, ~ 18 kcal/mol energy is available to the S_1 state after relaxation from S_2 , which is sufficient to explore a broad range of possible structures (the range of rotamer energies in the S_1 state is 13 kcal/mol). It has also been previously reported in Tr-XAS measurements that a Wigner distribution of vibrationally excited states was needed to appropriately match calculated X-ray spectra to experimental results.²⁹ It is possible that future work involving vibrationally excited trajectories may prove necessary to more accurately model the experimental S_1 state spectrum. We also note that OO-DFT predicts a lower intensity for the 286.1 eV peak in the experimental spectrum [as shown in Fig 5 a) and b)], and this discrepancy can possibly also be resolved by sampling over more geometries.

To obtain an experimental T_1 state spectrum for Figs. 5c) and 5d), the transient data from 5 to 30 ps were averaged and a portion (20%) of the S_0 state spectrum was added back under the assumption of a 20% excitation, thus simulating a “pure” triplet state. It is known that upon UV excitation the HfAcAc molecule is able to undergo rotation and form a number of rotational isomers (rotamers).⁵⁶ These rotamers involve rotations about the C_2-C_3 , $C_3=C_4$ and C_4-OH bonds, with each of these bonds either in “cis” (C) or “trans” (T) configurations.⁵⁶ The notation used in the literature consists of three letters describing the orientation for each bond. Chemical structures displaying these orientations are shown in Fig. S9. The ground state enol form shown in Fig 1 is the triple cis or CCC rotamer, which is strongly favored energetically at the S_0 state due to the hydrogen bond.

However, we find that the rotamer energies in the T_1 state differ by less than 2 kcal/mol from one another, significantly less than the ~ 44 kcal/mol energy gained following relaxation from the S_2 excited state. Nonplanar configurations like the twisted CCT/TCC/TCT forms therefore are quite accessible in the T_1 state. Indeed, the $^3\pi\pi^*$ character of the state permits relatively easy rotation about the C_3-C_4 bond, causing multiple non hydrogen bonded rotamers to collapse into the same, twisted, structure. For example, geometry optimization on the distinct TCT and TTT rotamers, on the T_1 state, lead to the same local minimum. Both the C=C bond and the hydrogen bond are broken in such twisted structures.

Fig. 5 c) shows that the experimental spectrum for the T_1 state has clear peaks at 281.7, 283.9, 286.8, 287.5 and 289.3 eV, in addition to some higher energy features. OO-DFT calculations find that all nonplanar rotamers of the T_1 state are predicted to have a very similar C K-edge spectrum (as shown in Fig. S9), and thus only the computed results for the TCT state are shown in Fig. 5 c). Experiment and theory agree fairly well with each other (especially for the features at 281.7, 283.9, 286.6, 289.3 eV), indicating that a large proportion of molecules in the T_1 state exist in hydrogen-bond cleaved, twisted forms.

Meanwhile, it can be seen that in Fig. 5d) the planar CCC form of the T_1 state does not adequately reproduce the experimental data on its own. Most notably, the peak at 283.9 eV has the calculated transition at 283.1 eV and is predicted to be of much weaker intensity. Agreement for the first peak at 281.7 eV however is good, and some of the higher energy features align relatively well with experiment (such as the one at 289.3 eV). Indeed, a comparison of Figs. 5c) and 5d) suggests that the T_1 state molecules may exist as a mixture of planar and twisted nonplanar forms. The computed spectra for different ratios of these planar and nonplanar forms are shown in Fig. S10, which reveals that significant features at 283.1 and 286 eV would be displayed if the proportion of planar molecules was in excess of $\sim 35\%$. These predicted transition energies are not directly overlapping with the experimentally observed peaks, thereby indicating that the majority of the molecules are likely present in a twisted form. This is not surprising, as there are a greater number

of nonplanar local minima than planar local minima for the T_1 state of HfAcAc, with the energy difference between these states being quite low relative to the energy available to the molecule.

In this regard, it is worth noting that while peak 1 (281.7 eV, first T_1 transition in Fig. 3) is nearly identical for the planar and non-planar rotamers, peak 2 (283.9 eV, second T_1 transition in Fig. 3) is not present in the planar CCC state. This suggests the rotation must occur rapidly along the potential energy surface since there is no observed delay in the experimental data between peaks 1 and 2 within the uncertainty of the measurements. We also note that the TCC rotamer has been suggested as a precursor to the transition state for the proposed photodissociation pathway to form HF + pentafluoromethyl-3-furanone.¹⁷

Despite this, the possible pentafluoromethyl-3-furanone (PF3F) product, is not observed in the experimental spectrum. The PF3F molecule in the S_0 ground state is predicted by ROKS to have a C K-edge spectrum very similar to HfAcAc ground state (as shown in Fig. S6). Therefore, formation of the S_0 state PF3F would lead to a decay in the T_1 signals and reduction in the ground state bleach. However, such behavior is not clearly evident in the experimental data and the transient spectrum remains virtually constant from 5-30 ps (as shown in Fig. S5). Given the signal-to-noise ratio of the experiment, even a 15% conversion of T_1 HfAcAc into the S_0 PF3F product should be readily observable. The PF3F could potentially form in the T_1 state as well, and the computed spectrum for this electronic state is very similar to the CCC form of HfAcAc in the T_1 state shown in Fig. 5 d). Formation of the T_1 state PF3F therefore should correspond to a depletion in peak 2 over time, as nonplanar T_1 HfAcAc would be consumed to produce PF3F. No obvious decay in peak 2 is observed, indicating that a significant amount of PF3F is not forming on the timescales studied in this experiment, given the signal-to-noise ratio of the setup. Indeed, the lack of decrease in triplet intensity over the experimental timescales suggests that the lifetime of the triplet is significantly longer than 30 ps. This indicates that the relaxation back to the ground state from the triplet is delayed and any photoproducts may occur at longer

timescales.

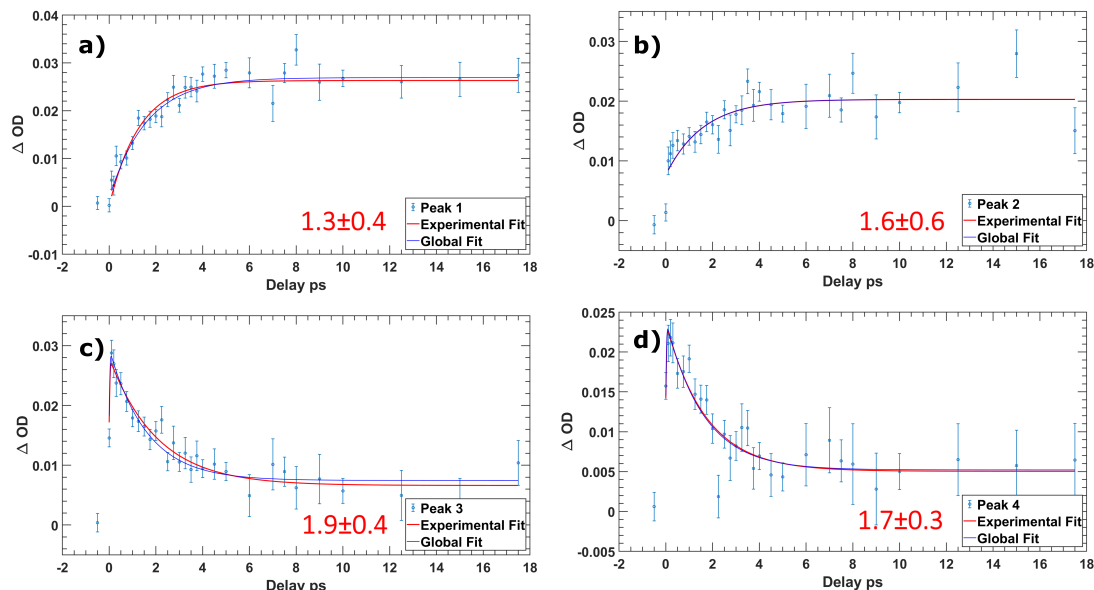


Figure 6: Fits for peaks 1-4, each consisting of an individual exponential fit corresponding to each peak and a 1.6 ± 0.4 ps exponential determined via global fitting, both are convoluted with the IRF.

Fig. 6 illustrates the various time evolutions of the features in the experimental data. Each of these were fit with an exponential and a Gaussian error function to incorporate the instrument response function (IRF) of 80 fs. A global fitting routine was used to determine the fit with a single exponential for peaks 1-4. It was determined that an exponential with a time constant of 1.6 ± 0.4 ps corresponds to the intersystem crossing from the S_1 state to the T_1 state. Somewhat surprisingly there is only a minor change in the rate of the intersystem crossing when compared to AcAc, where a S_1 lifetime of 1.5 ps was measured. It should be noted that the features showing the clearest signal correspond to the central three carbon atoms. These central carbon atoms are part of the π backbone, which extends to the two oxygen atoms. In the transient data there are no clear changes in the high energy carbon peaks that occur on the timescale of the intersystem crossing. This indicates that the CF_3 carbons do not play a large role in this conversion from S_1 to T_1 , which is mostly driven by the π system composed of the central C atoms and the O atoms. This raises the question whether a hypothetical electron withdrawing or donating group attached to the central C_3

carbon atom would produce a significant change in the rate of intersystem crossing. This substitution could have a more significant effect on the conjugated π system present on the acetylacetone backbone.

Additional fitting for peaks 5-6 is shown in the supporting information; the fits of peaks 5 and 6 reinforce the rate constants determined by the fit performed for peaks 1-4 and support the two step kinetic model. There are also higher energy peaks that appear to correspond to processes faster than intersystem crossing, which are discussed further in the supporting information.

Conclusions

Time-resolved X-ray absorption spectroscopy was used to investigate the non-adiabatic relaxation dynamics of hexafluoro-acetylacetone following 266 nm excitation. It was found that the intersystem crossing between the $S_1 \rightarrow T_1$ occurs in 1.6 ± 0.4 ps. OO-DFT calculations are used to assign features of the C K-edge spectra of the S_0 , S_1 and T_1 states, and also aid in determining that hydrogen bond cleavage occurs prior to/immediately following the intersystem crossing from the singlet S_1 to the T_1 state. The T_1 state is therefore present as a mixture of rotational isomers (rotamers). Additionally, it was determined that even the S_1 state is present over a range of geometries, with OO-DFT calculations illustrating the effect of the dihedral angle on the predicted positions of the $1s \rightarrow \pi^*$ transitions.

It was observed that the substitution of multiple fluorine atoms does not significantly impact the intersystem crossing rate between the singlet S_1 and triplet T_1 states in HfAcAc compared to AcAc. However the addition of these fluorine atoms significantly blueshifts the ionization continuum of the carbon K-edge, emphasizing higher energy features in the time-resolved spectra and allowing more possible states to be observed. The large shifts observed through the different chemical environments surrounding the various carbon atoms opens the doorway to studying different fluorinated species where these shifts may simplify

the XAS spectra of other prototypical molecules.

The dynamics relating to crossing between the S_2 and S_1 states could not be resolved in this experiment due to a combination of limited experimental temporal resolution and similarity between the expected spectra of the S_2 and S_1 states. In the future, experiments at the oxygen K-edge may provide more insights regarding this transition; this is because there are larger differences in spectra expected in the oxygen region of the singlet excited states.⁵⁷

We demonstrate that time-resolved X-ray absorption spectroscopy using a broadband carbon K-edge high-harmonic probe reveals an ultrafast intersystem crossing between the S_1 and T_1 states in HfAcAc. Elucidation of the roles played by S_2 and T_2 states remain to be identified by measurements at a faster time resolution. Overall, these results further reinforce the applicability of time-resolved X-ray absorption spectroscopy and its ability to act as a powerful probe to elucidate non-adiabatic dynamics in photoexcited molecules.

Conflicts of interest

The authors declare the following competing interest: M.H.-G is a part-owner of Q-Chem, which is the software platform in which the quantum chemical calculations were carried out.

Supporting Information

The supporting information provides further details regarding the experimental methods, power dependence studies, experimental results regarding high energy channels, shorter and longer time dynamics than shown in the primary publication, additional theoretical calculations regarding possible photoproducts and electronic states of interest.

Acknowledgement

This research was supported by Director, Office of Science, Office of Basic Energy Sciences, of the U.S. Department of Energy under Contract No. DE-AC02-05CH11231, through the Gas Phase Chemical Physics program (E.A.H, V.S, T.X, S. R. L.) and Atomic, Molecular, and Optical Sciences program (D.H. and M.H.G.). The authors would also like to acknowledge Paul Houston for his achievements in physical chemistry throughout the years and how his contributions to the field have helped shape the directions of future research.

References

- (1) Kukura, P.; McCamant, D. W.; Yoon, S.; Wandschneider, D. B.; Mathies, R. A. Structural Observation of the Primary Isomerization in Vision with Femtosecond-Stimulated Raman. *Science* **2005**, *310*, 1006–1009.
- (2) Pederzoli, M.; Pittner, J.; Barbatti, M.; Lischka, H. Nonadiabatic Molecular Dynamics Study of the cis–trans Photoisomerization of Azobenzene Excited to the S1 State. *The Journal of Physical Chemistry A* **2011**, *115*, 11136–11143.
- (3) Mar, T.; Govindjee,; Singhal, G.; Merkelo, H. Lifetime of the Excited State In Vivo: I. Chlorophyll a in Algae, at Room and at Liquid Nitrogen Temperatures; Rate Constants of Radiationless Deactivation and Trapping. *Biophysical Journal* **1972**, *12*, 797–808.
- (4) Maeda, S.; Taketsugu, T.; Ohno, K.; Morokuma, K. From Roaming Atoms to Hopping Surfaces: Mapping Out Global Reaction Routes in Photochemistry. *Journal of the American Chemical Society* **2015**, *137*, 3433–3445.
- (5) Stolow, A.; Bragg, A. E.; Neumark, D. M. Femtosecond Time-Resolved Photoelectron Spectroscopy. *Chemical Reviews* **2004**, *104*, 1719–1758.

- (6) Siwick, B. J.; Dwyer, J. R.; Jordan, R. E.; Miller, R. J. D. An Atomic-Level View of Melting Using Femtosecond Electron Diffraction. *Science* **2003**, *302*, 1382–1385.
- (7) Wolf, T. J. A. et al. Probing ultrafast $\pi\pi^*/n\pi^*$ internal conversion in organic chromophores via K-edge resonant absorption. *Nature Communications* **2017**, *8*, 29.
- (8) Squibb, R. J. et al. Acetylacetone photodynamics at a seeded free-electron laser. *Nature Communications* **2018**, *9*, 63.
- (9) Kotsina, N.; Candelaresi, M.; Saalbach, L.; Zawadzki, M. M.; Crane, S. W.; Sparling, C.; Townsend, D. Short-wavelength probes in time-resolved photoelectron spectroscopy: an extended view of the excited state dynamics in acetylacetone. *Phys. Chem. Chem. Phys.* **2020**, *22*, 4647–4658.
- (10) Bhattacharjee, A.; Pemmaraju, C. D.; Schnorr, K.; Attar, A. R.; Leone, S. R. Ultrafast Intersystem Crossing in Acetylacetone via Femtosecond X-ray Transient Absorption at the Carbon K-Edge. *Journal of the American Chemical Society* **2017**, *139*, 16576–16583, Publisher: American Chemical Society.
- (11) Kawaguchi, S. Variety in the coordination modes of β -dicarbonyl compounds in metal complexes. *Coordination Chemistry Reviews* **1986**, *70*, 51–84.
- (12) Shaath, N. A. Ultraviolet filters. *Photochem. Photobiol. Sci.* **2010**, *9*, 464–469.
- (13) Zhang, G.; Wu, B.; Zhang, S. Effects of acetylacetone on the photoconversion of pharmaceuticals in natural and pure waters. *Environmental pollution (Barking, Essex : 1987)* **2017**, *225*, 691–699.
- (14) Bassett, J. E.; Whittle, E. The photochemistry of hexafluoroacetylacetone in the vapour phase. Occurrence of a novel HF elimination reaction. *International Journal of Chemical Kinetics* **1976**, *8*, 859–876.

- (15) Yoon, M.-C.; Choi, Y. S.; Kim, S. K. The OH Product State Distribution from the Photodissociation of Hexafluoroacetylacetone. *The Journal of Physical Chemistry A* **2000**, *104*, 4352–4355.
- (16) Chen, X.-B.; Fang, W.-H.; Phillips, D. L. Theoretical Studies of the Photochemical Dynamics of Acetylacetone: Isomerization, Dissociation, and Dehydration Reactions. *The Journal of Physical Chemistry A* **2006**, *110*, 4434–4441.
- (17) Muyskens, K. J.; Alsum, J. R.; Thielke, T. A.; Boer, J. L.; Heetderks, T. R.; Muyskens, M. A. Photochemistry of UV-Excited Trifluoroacetylacetone and Hexafluoroacetylacetone I: Infrared Spectra of Fluorinated Methylfuranones Formed by HF Photoelimination. *The Journal of Physical Chemistry A* **2012**, *116*, 12305–12313.
- (18) Reiffers, A.; Torres Ziegenbein, C.; Engelhardt, A.; Kühnemuth, R.; Gilch, P.; Czekeilius, C. Impact of Mono-Fluorination on the Photophysics of the Flavin Chromophore. *Photochemistry and Photobiology* **2018**, *94*, 667–676.
- (19) Bracker, M.; Dinkelbach, F.; Weingart, O.; Kleinschmidt, M. Impact of fluorination on the photophysics of the flavin chromophore: a quantum chemical perspective. *Phys. Chem. Chem. Phys.* **2019**, *21*, 9912–9923, Publisher: The Royal Society of Chemistry.
- (20) Uoyama, H.; Goushi, K.; Shizu, K.; Nomura, H.; Adachi, C. Highly efficient organic light-emitting diodes from delayed fluorescence. *Nature* **2012**, *492*, 234–238.
- (21) Zhang, Q.; Li, B.; Huang, S.; Nomura, H.; Tanaka, H.; Adachi, C. Efficient blue organic light-emitting diodes employing thermally activated delayed fluorescence. *Nature Photonics* **2014**, *8*, 326–332.
- (22) Chatterjee, C.; Incarvito, C. D.; Burns, L. A.; Vaccaro, P. H. Electronic Structure and Proton Transfer in Ground-State Hexafluoroacetylacetone. *The Journal of Physical Chemistry A* **2010**, *114*, 6630–6640.

- (23) De Vries, B.; Muyskens, M. Fluorine atom influence on intramolecular hydrogen bonding, isomerization and methyl group rotation in fluorinated acetylacetones. *Computational and Theoretical Chemistry* **2016**, *1097*, 15–24.
- (24) Nakanishi, H.; Morita, H.; Nagakura, S. Electronic Structures and Spectra of the Keto and Enol Forms of Acetylacetone. *Bulletin of the Chemical Society of Japan* **1977**, *50*, 2255–2261.
- (25) Nakanishi, H.; Morita, H.; Nagakura, S. Charge-Transfer Character in the Intramolecular Hydrogen Bond: Vacuum Ultraviolet Spectra of Acetylacetone and Its Fluoro Derivatives. *Bulletin of the Chemical Society of Japan* **1978**, *51*, 1723–1729.
- (26) Antonov, I.; Voronova, K.; Chen, M.-W.; Sztáray, B.; Hemberger, P.; Bodi, A.; Osborn, D. L.; Sheps, L. To Boldly Look Where No One Has Looked Before: Identifying the Primary Photoproducts of Acetylacetone. *The Journal of Physical Chemistry A* **2019**, *123*, 5472–5490, PMID: 31241939.
- (27) Kusaba, M.; Tsunawaki, Y. Production of CO by UV irradiation of acetylacetone. *Radiation Physics and Chemistry* **2007**, *76*, 1447–1449, Proceedings of the 11th Tihany Symposium on Radiation Chemistry.
- (28) Yang, Z.; Schnorr, K.; Bhattacharjee, A.; Lefebvre, P.-L.; Epshtein, M.; Xue, T.; Stanton, J. F.; Leone, S. R. Electron-Withdrawing Effects in the Photodissociation of CH₂ICl To Form CH₂Cl Radical, Simultaneously Viewed Through the Carbon K and Chlorine L_{2,3} X-ray Edges. *Journal of the American Chemical Society* **2018**, *140*, 13360–13366.
- (29) Scutelnic, V.; Tsuru, S.; Pápai, M.; Yang, Z.; Epshtein, M.; Xue, T.; Haugen, E.; Kobayashi, Y.; Krylov, A. I.; Møller, K. B.; Coriani, S.; Leone, S. R. X-ray transient absorption reveals the 1Au ($n\pi^*$) state of pyrazine in electronic relaxation. *Nature Communications* **2021**, *12*, 5003.

- (30) Fu, Y.; Nishimura, K.; Shao, R.; Suda, A.; Midorikawa, K.; Lan, P.; Takahashi, E. J. High efficiency ultrafast water-window harmonic generation for single-shot soft X-ray spectroscopy. *Communications Physics* **2020**, *3*, 92.
- (31) Pertot, Y.; Schmidt, C.; Matthews, M.; Chauvet, A.; Huppert, M.; Svoboda, V.; von Conta, A.; Tehlar, A.; Baykusheva, D.; Wolf, J.-P.; Wörner, H. J. Time-resolved x-ray absorption spectroscopy with a water window high-harmonic source. *Science* **2017**, *355*, 264–267.
- (32) Ross, A. D.; Hait, D.; Scutelnic, V.; Haugen, E. A.; Ridente, E.; Balkew, M. B.; Neumark, D. M.; Head-Gordon, M.; Leone, S. R. Jahn-Teller distortion and dissociation of CCl₄⁺ by transient X-ray spectroscopy simultaneously at the carbon K- and chlorine L-edge. *Chem. Sci.* **2022**, –.
- (33) Loh, Z.-H.; Leone, S. R. Capturing Ultrafast Quantum Dynamics with Femtosecond and Attosecond X-ray Core-Level Absorption Spectroscopy. *The Journal of Physical Chemistry Letters* **2013**, *4*, 292–302.
- (34) Hait, D.; Head-Gordon, M. Orbital optimized density functional theory for electronic excited states. *J. Phys. Chem. Lett.* **2021**, *12*, 4517–4529.
- (35) Attar, A. R.; Bhattacharjee, A.; Pemmaraju, C.; Schnorr, K.; Closser, K. D.; Prendergast, D.; Leone, S. R. Femtosecond x-ray spectroscopy of an electrocyclic ring-opening reaction. *Science (New York, N.Y.)* **2017**, *356*, 54–59.
- (36) Epshtein, M.; Scutelnic, V.; Yang, Z.; Xue, T.; Vidal, M. L.; Krylov, A. I.; Coriani, S.; Leone, S. R. Table-Top X-ray Spectroscopy of Benzene Radical Cation. *The Journal of Physical Chemistry A* **2020**, *124*, 9524–9531.
- (37) Sairanen, O.-P.; Kivimäki, A.; Nõmmiste, E.; Aksela, H.; Aksela, S. High-resolution pre-edge structure in the inner-shell ionization threshold region of rare gases Xe, Kr, and Ar. *Phys. Rev. A* **1996**, *54*, 2834–2839.

- (38) Epifanovsky, E., et al. Software for the frontiers of quantum chemistry: An overview of developments in the Q-Chem 5 package. *J. Chem. Phys.* **2021**, *155*, 084801.
- (39) Sun, J.; Ruzsinszky, A.; Perdew, J. P. Strongly Constrained and Appropriately Normed Semilocal Density Functional. *Phys. Rev. Lett.* **2015**, *115*, 036402.
- (40) Frank, I.; Hutter, J.; Marx, D.; Parrinello, M. Molecular dynamics in low-spin excited states. *J. Chem. Phys.* **1998**, *108*, 4060–4069.
- (41) Kowalczyk, T.; Tsuchimochi, T.; Chen, P.-T.; Top, L.; Van Voorhis, T. Excitation energies and Stokes shifts from a restricted open-shell Kohn-Sham approach. *J. Chem. Phys.* **2013**, *138*, 164101.
- (42) Hait, D.; Oosterbaan, K. J.; Carter-Fenk, K.; Head-Gordon, M. Computing x-ray absorption spectra from linear-response particles atop optimized holes. *J. Chem. Phys.* **2022**, *156*, 201104.
- (43) Bagus, P. S. Self-consistent-field wave functions for hole states of some Ne-like and Ar-like ions. *Phys. Rev.* **1965**, *139*, A619–A634.
- (44) Besley, N. A.; Gilbert, A. T.; Gill, P. M. W. Self-consistent-field calculations of core excited states. *J. Chem. Phys.* **2009**, *130*, 124308.
- (45) Hait, D.; Haugen, E. A.; Yang, Z.; Oosterbaan, K. J.; Leone, S. R.; Head-Gordon, M. Accurate prediction of core-level spectra of radicals at density functional theory cost via square gradient minimization and recoupling of mixed configurations. *The Journal of Chemical Physics* **2020**, *153*, 134108, Publisher: American Institute of Physics.
- (46) Hait, D.; Head-Gordon, M. Highly Accurate Prediction of Core Spectra of Molecules at Density Functional Theory Cost: Attaining Sub-electronvolt Error from a Restricted Open-Shell Kohn–Sham Approach. *The Journal of Physical Chemistry Letters* **2020**, *11*, 775–786.

- (47) Hait, D.; Head-Gordon, M. Excited State Orbital Optimization via Minimizing the Square of the Gradient: General Approach and Application to Singly and Doubly Excited States via Density Functional Theory. *Journal of Chemical Theory and Computation* **2020**, *16*, 1699–1710, PMID: 32017554.
- (48) Barca, G. M.; Gilbert, A. T.; Gill, P. M. W. Simple Models for Difficult Electronic Excitations. *J. Chem. Theory Comput.* **2018**, *14*, 1501–1509.
- (49) Ambrose, M. A.; Jensen, F. Probing Basis Set Requirements for Calculating Core Ionization and Core Excitation Spectroscopy by the Δ Self-Consistent-Field Approach. *J. Chem. Theory Comput.* **2018**, *15*, 325–337.
- (50) Jensen, F. Unifying general and segmented contracted basis sets. Segmented polarization consistent basis sets. *J. Chem. Theory Comput.* **2014**, *10*, 1074–1085.
- (51) Chai, J.-D.; Head-Gordon, M. Long-range corrected hybrid density functionals with damped atom–atom dispersion corrections. *Phys. Chem. Chem. Phys.* **2008**, *10*, 6615–6620.
- (52) Liang, J.; Feng, X.; Hait, D.; Head-Gordon, M. Revisiting the performance of time-dependent density functional theory for electronic excitations: Assessment of 43 popular and recently developed functionals from rungs one to four. *Journal of Chemical Theory and Computation*
- (53) Hirata, S.; Head-Gordon, M. Time-dependent density functional theory within the Tamm–Dancoff approximation. *Chem. Phys. Lett.* **1999**, *314*, 291–299.
- (54) Hait, D.; Rettig, A.; Head-Gordon, M. Beyond the Coulson–Fischer point: characterizing single excitation CI and TDDFT for excited states in single bond dissociations. *Phys. Chem. Chem. Phys.* **2019**, *21*, 21761–21775.

- (55) Géneaux, R.; Chang, H.-T.; Schwartzberg, A. M.; Marroux, H. J. B. Source noise suppression in attosecond transient absorption spectroscopy by edge-pixel referencing. *Opt. Express* **2021**, *29*, 951–960.
- (56) Nagashima, N.; Kudoh, S.; Nakata, M. Infrared and UV–visible absorption spectra of hexafluoroacetylacetone in a low-temperature argon matrix. I. Structure of a non-chelated enol-type isomer. *Chemical Physics Letters* **2003**, *374*, 59–66.
- (57) Faber, R.; Kjønstad, E. F.; Koch, H.; Coriani, S. Spin adapted implementation of EOM-CCSD for triplet excited states: Probing intersystem crossings of acetylacetone at the carbon and oxygen K-edges. *The Journal of Chemical Physics* **2019**, *151*, 144107.